

# WET AND DRY CUP TEST WITH HYGROSCOPIC MATERIALS: WHAT DO WE REALLY MEASURE

Yuliang Zou , Eléa Moss , Laurent Brochard , Philippe Coussot 

*Laboratoire Navier (Ecole des Ponts Paris Tech-Univ Gustave Eiffel-CNRS), Champs-sur-Marne, France*

**Correspondence to:**

Philippe Coussot,  
[philippe.coussot@univ-eiffel.fr](mailto:philippe.coussot@univ-eiffel.fr)

**How to Cite:**

Zou, Y., Moss, E., Brochard, L., & Coussot, P. Wet and dry cup test with hygroscopic materials: what do we really measure? InterPore Journal, 1(2), ipj240824–4.  
<https://doi.org/10.69631/ipj.v1i2nr22>

RECEIVED: 28 Jan. 2024

ACCEPTED: 6 June 2024

PUBLISHED: 24 Aug. 2024

**ABSTRACT**

Wet and dry cup tests are widely used to characterize the vapor permeability (or the apparent vapor diffusion coefficient) of construction materials. From a theoretical approach, we examined the transport characteristics of such tests in detail. We precisely quantified the impact of the boundary conditions on the apparent diffusion coefficient and the time required to reach steady-state conditions, which is critical for accurate estimation of this coefficient. Finally, a major point concerns the physical meaning of the value measured through this type of test. For a homogeneous non-hygroscopic medium, the diffusion coefficient obtained represents the diffusion coefficient of vapor through the medium. For hygroscopic materials, where vapor diffusion, bound water diffusion, and sorption or desorption processes may be encountered, we demonstrate that the total water transport diffusion coefficient in the medium is strongly different from, yet proportional to, the apparent vapor diffusion coefficient. We validated and illustrated this analysis based on experiments with cellulose fiber stacks of different porosities and under different experimental conditions.

**KEYWORDS**

Water transport diffusion, Boundary conditions, Hygroscopic materials, Wet cup test, Dry cup test



©2024 The Authors

This is an open access article published by InterPore under the terms of the Creative Commons Attribution-NonCommercial-NoDerivatives 4.0 International License (CC BY-NC-ND 4.0) (<https://creativecommons.org/licenses/by-nc-nd/4.0/>).

## 1. INTRODUCTION

Bio-based construction materials are typically stacks of natural fibers (or bio-elements) derived from wood, wheat, jute, flax, bamboo, straw, coir, cotton, pulp, etc., and are mainly used for insulation, or dispersions of vegetal elements (wood, hemp, cellulose wadding, straw, etc.) coated with a mineral matrix (lime, cement, earth, plaster, clay, etc.) generally used as filling for walls, but also for insulation, such as hemp concrete, wood concrete, flax concrete, adobe, and cob. The use of such materials is recognized (1, 9, 11) as a means of overcoming many of the issues related to increasing carbon dioxide emissions from construction through (i) their sustainable production as crops grown annually or as longer harvest-cycle forestry due to the significant reduction of CO<sub>2</sub> emissions during their production, their contribution to air quality, and the reduction of energy consumption for heating or cooling. The latter qualities are obtained through exchanges between water vapor and “bound water,” i.e., water absorbed in the solid structure combined with heat transfer. Consequently, understanding and predicting the water

and heat (hygrothermal) transfers in such materials is essential for selecting them appropriately, adjusting their conditions of use, and designing innovative materials. The current analysis of their performance is generally based on evaluations at a global scale (5, 7, 10, 13, 26) or continuous models (8, 12, 15, 17, 18, 20, 23, 24, 25) that rely on various parameters; however, some of them can hardly be identified from independent measurements.

In this context, a basic characteristic of these materials is their resistance to vapor transport through the material, which, at first sight, corresponds to a straightforward property of the material and can be determined from simple experiments. The standard approach (2, 3) consists of imposing a humidity gradient between the two faces of a sample and measuring the resulting flux of water extracted from the upper surface in the steady state. The lower sample surface is at some distance from the water layer or desiccant, and the upper sample surface is placed in the ambient air of a climatic chamber or under some air flow. The apparent resistance to vapor transport is then proportional to the ratio of the humidity gradient to the water flux. One can also define permeability, which is proportional to the inverse ratio.

This test is widely used; however, its relevance has often been discussed. It was noted in the book edited by Trechsel (22) that the permeability to vapor deduced from such measurements depends not only on the range covered by the humidity gradient, but also on the operator and the entire experimental system used. One may question both the relevance of the technique itself and the validity of the test for determining intrinsic properties of the material.

The first problem identified by Trechsel (22) is that the permeability to vapor may depend on the range of relative humidities involved in the test. To address this problem at least partly, the standard approach consists of examining two average permeabilities associated with two different ranges: low humidity (dry cup method) and high humidity (wet cup method). Petersen et al. (19) suggested to further address the problem by using a series of dry cup and wet cup tests associated with ranges of humidities allowing to cover more precisely the full range.

Another aspect is the boundary conditions of the test. The boundary condition along the sample bottom is associated with a well-defined system: the vapor diffuses between two surfaces (the sample bottom and desiccant or water bath) through still air. However, it was observed that, with a desiccant, the measured relative humidity in this region may differ from the expected one, resulting in relative errors ranging from 5% to 450% in the predicted vapor permeability value (4).

The boundary condition along the top of the sample appears to be even more problematic. This is because some air flow can now exist along the sample surface (4). The boundary condition is described with the help of a mass transfer coefficient, which may be seen as the inverse of an additional resistance to vapor flux owing to the interaction of the surface with the airflow (4, 21). Seng et al. (21) reviewed different expressions proposed in the literature and suggested the use of an average value. However, these authors (4, 21) also observed that the experimental conditions (air velocity and sample thickness) and the calculation method have an impact on the permeability estimation. Finally, Mustapha et al. (16) suggested an original method for determining the mass transfer coefficient, which consists of measuring at the same time the water flux extracted from a wet cup in which the sample is replaced by water and subjected to the same air flux. The coefficient was then deduced from the mass flux from the pure water surface. The fundamental assumption in this context is that this coefficient depends only on the air flux characteristics along the surface, and not on the material characteristics.

A last remark here concerns the procedure for determining the steady-state vapor flux. Because the initial conditions are typically a sample prepared under a specific relative humidity (RH), its water content is homogeneous in the sample, which does not correspond to the conditions in the steady state during the wet or dry cup test. Consequently, there is a transient period during which the distribution of RH evolves, and a steady state is reached when this distribution is stabilized. In the ISO norm (3), recommendations concerning the conditions for reaching a steady state are vague. It is suggested to "weigh the sample at time intervals selected according to the specimen characteristics. . . until five successive determinations of change in mass per weighing interval are constant within 5% of the mean

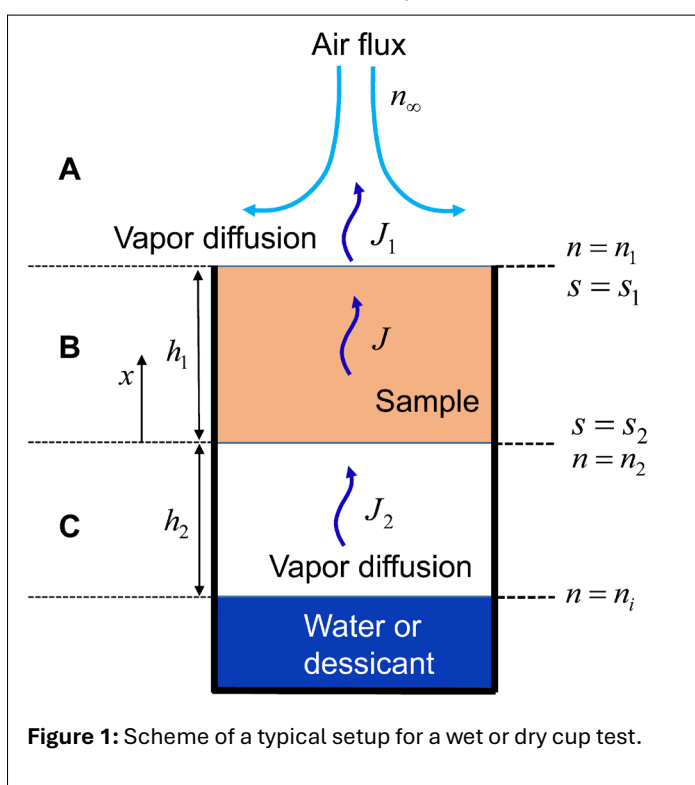
value. . . ". Such an approach seems arbitrary, and because the exact dynamics depend on the detailed properties of the material and the characteristics of the setup (sample thickness and air flux velocity), we can suspect that it would allow us to obtain the effective value of permeability only by chance.

Finally, the ultimate question concerns the physical meaning of the measured value through this type of test. For a homogeneous non-hygroscopic medium, the diffusion coefficient deduced from the wet or dry cup tests represents the diffusion coefficient of vapor through the medium. However, for materials in which one may encounter, in addition to vapor diffusion, some bound water diffusion, and some sorption or desorption processes, it does not seem obvious to relate the outgoing vapor flux to the internal water transport properties of the material. Here, we review in detail the physics of the wet or dry cup test, including the different processes occurring inside, above, and below the sample, to properly quantify various aspects of the problem. Additionally, owing to some recent approaches to the detailed transport properties in such media, we also analyze the physical meaning of the diffusion coefficient value deduced from such tests. We start by considering the basic simplified approach from which we derive the dynamics, thus providing a straightforward criterion for estimating the time necessary to reach a steady state. In the next step, we describe the boundary conditions along the top surface of the sample in detail, based on a rigorous continuum mechanics approach. Finally, we analyze the physical processes occurring inside the hygroscopic sample that play a role in water transport.

## 2. THEORY

Let us consider the typical setup as illustrated in **Figure 1**: a sample of thickness  $h_1$  (region B) along the axis of the system  $x$ , sealed to the walls of a container with either a distilled water bath, a desiccant or a water-salt solution, whose free surface is at a distance  $h_2$  (region C) from the sample bottom, and tending to impose a RH  $n_i$ ; the upper sample surface is in contact with the ambient air (region A) in a climatic chamber assumed to be maintained at a RH  $n_\infty$ . However, regardless of the exact conditions in the environment of the sample surface, maintaining a given value of RH implies that there is some renewal of the ambient air and thus some air flux (29). Therefore, we represent some air flux along the sample surface (see **Fig. 1**). As a corollary, well-controlled boundary conditions correspond to a fixed air flux (regardless of its intensity) for a given RH value (29). The sample was initially in a homogeneous state of humidity, reached after being left for a sufficient time in air at a RH  $n_0$ .

Generally, the RH at the bottom of region C, i.e.,  $n_i$ , differs from the RH in region A, i.e.,  $n_\infty$ , and these regions are separated by a porous medium, the system is not at equilibrium, and we expect a transport of water between region C and region A. This transport occurs in the form of vapor at least in regions A and C, i.e., through air. Moreover, if we can neglect the resulting variations over time of the characteristics of the system imposing the humidity in region C, we expect to reach a steady-state transport after some time. In this steady-state regime, the vapor mass flux  $J$  through the surface just above the top of the sample was constant. The way water is transported through region B, i.e., through the sample, may be more complex and will be discussed below. However, in the framework of the standard approach (2), this transport is



considered to be a vapor flow through the material, induced by the difference in the partial pressure of vapor ( $p_v$ ) between the bottom and top of the sample. This leads to the characterization of the sample by defining the water vapor permeability (2) as shown in **Equation 1**, where  $p_v$  is the water vapor pressure, which can be written as  $p_v = np_0$ , with  $p_0$  representing the saturation vapor pressure at the test temperature.

$$k = -\frac{Jh_1}{\Delta p_v} \quad (1)$$

In fact, because vapor transport fundamentally results from a gradient of water concentration over the sample thickness, we are dealing with a diffusion process along the sample axis, which is described in a general way by Fick's law in the one-dimensional form (**Eq. 2**), where  $D^*$  is the apparent diffusion coefficient of vapor through the sample, and  $p_0$  is the saturation vapor density.

$$J = -\rho_0 D^* \frac{\partial n}{\partial x} \quad (2)$$

The basic calculation (see 2) assumes that just below the sample, the RH is equal to  $n_i$ , while just above the sample, it is equal to  $n_\infty$ , i.e.,  $n_1 = n_\infty$  and  $n_2 = n_i$ . Owing to the mass conservation (in the steady state),  $J$  is constant along the axis  $x$ . If the diffusion coefficient is constant throughout the sample, we deduce from **Equation 2** that  $(\partial n/\partial x)$  is constant along the sample thickness, which means that RH varies linearly along  $x$ , and  $(\partial n/\partial x)$  is equal to  $\Delta n/h_1 = (n_\infty - n_i/h_1)$ . Finally, we deduce a simple expression for the diffusion coefficient (**Eq. 3**), which can be computed directly by measuring the steady-state mass flux  $J$ .

$$D^* = \frac{J}{\rho_0} \frac{h_1}{n_i - n_\infty} \quad (3)$$

Recall that this expression relies on the following assumptions: steady state has been reached, relative humidity is imposed along the sample surfaces, and the diffusion coefficient of vapor is constant in the material. Moreover, this expression defines a transport diffusion coefficient that does not distinguish between different transport processes inside the medium. In the following section, we discuss these aspects.

Since  $\Delta p_v = (n_\infty - n_i)p_0$ , **Equations 1** and **3** express a linear relationship between  $J$  and  $(n_\infty - n_i)$ , and we deduce that  $k = \rho_0 D^*/\rho_0$ . Considering the expression for the saturation vapor pressure  $p_0 = \rho_0 RT/M$ , in which  $R = 8.314 \text{ J mol}^{-1}\text{K}^{-1}$  is the ideal gas constant,  $M = 18 \text{ g mol}^{-1}$  is the molar mass of water molecules, and  $T$  is the temperature, this relation is then rewritten as  $k = (M/RT)D^*$ . Because permeability, as defined above, is simply proportional to the diffusion coefficient  $D^*$ , we focused on the characterization of the diffusion process, which is more physically sound, keeping in mind that the standard approach provides basic tools for determining a parameter proportional to  $D^*$ .

We have seen above that in the steady state, and under the assumption of a constant diffusion coefficient, the gradient of RH is constant throughout the material. Therefore, using the basic boundary conditions ( $n_1 = n_\infty$  and  $n_2 = n_i$ ), we have **Equation 4**:

$$n(x) = n_i + (n_\infty - n_i) \frac{x}{h_1} \quad (4)$$

In the steady state, the local value of  $n$ , i.e.,  $n(x)$ , is thus constant; therefore, after a sufficiently long time, the moisture content (MC) in the solid phase will be at equilibrium with this RH. Note that this distribution does not depend on the value of the diffusion coefficient as long as it remains constant over the range of MC resulting from the RH at the boundaries, i.e.,  $n_\infty$  and  $n_i$ .

## 2.1. Physical meaning of $D^*$

For a simple medium in which only vapor transport is possible, i.e., for a non-hygroscopic material, the measurement of the diffusion coefficient  $D^*$  can be used directly to describe the water transport inside

the medium under transient conditions. This is described by Fick's second law, which follows from mass conservation (Eq. 5):

$$\frac{\partial n}{\partial t} = -\frac{\partial}{\partial x}(D^*(\partial n/\partial x)) \quad (5)$$

However, we considered hygroscopic materials that can also contain bound water. When a hygroscopic material is placed at a given relative humidity, it absorbs some amount of water, which is described as the MC, i.e., the ratio of the absorbed water mass to the sample dry mass, which we denote here as  $s$ . At equilibrium and at a given temperature, this MC is a function of the relative humidity, which we write as  $s = f(n)$ , and refer to as the sorption curve. This quantifies the hygroscopicity of a material. Under these conditions and in the steady state, the distribution of MC in the sample can be deduced from the spatial distribution for  $n$  (Eq. 4), and from the sorption curve of the material, which is written as  $s(x) = s(n(x))$ . Note that the variables  $n$  and  $s$  directly quantify the water mass, as the bound water mass per unit volume is written as  $\rho_s s$ , in which  $\rho_s = 1500 \text{ kg m}^{-3}$  is the dry cellulose density, and the water vapor mass per unit volume is written as  $\rho_0 n$ . It is also worth noting that  $f$  can often be approximated within 10% using two linear functions of slope  $\alpha$  (see Discussion).

Thus, with hygroscopic materials, we expect exchanges between the vapor and bound water if equilibrium is not exactly reached locally. Moreover, we can even have significant transport of bound water inside the solid network. The existence of this transport was demonstrated in a recent work from desorption tests of cellulose fiber stacks filled with oil (27), and it was possible to fully dry initially bound water-saturated samples, indicating that the bound water diffuses along each fiber and jumps from one fiber to another in contact with it up to the free surface. Moreover, it was shown that at sufficiently low porosities and/or at high RH (28), bound water transport is dominant over vapor transport.

These effects must be considered for a proper description of transient processes. Let us consider the simple case of a transport along the direction  $x$  in a channel of constant cross-section area ( $A$ ). Mass conservation indicates that the variation in water mass during a brief time in a channel portion of length  $dx$  will be equal to the difference between the entering and exiting water fluxes. From the description of the total water flux and using Equation 2, we deduce that the water mass variation due to the flux difference is written as  $-\rho_0 A d(D^*(\partial n/\partial x))$ . The total mass of water in the channel portion is the sum of the vapor mass in the porosity  $\varepsilon$  i.e.,  $\rho_0 \varepsilon n A dx$ , and the bound water mass, i.e.,  $\rho_s (1 - \varepsilon) s A dx$ , so that the mass conservation can be written as shown in Equation 6:

$$\rho_0 \varepsilon \frac{\partial n}{\partial t} + \rho_s (1 - \varepsilon) \frac{\partial s}{\partial t} = -\rho_0 \frac{\partial}{\partial x} \left( D^* \frac{\partial n}{\partial x} \right) \quad (6)$$

The first term on the left-hand side is negligible compared to the second term because  $\rho_0 \ll \rho_s$ .

To obtain an equation involving only one variable, it is necessary to assume "instantaneous sorption equilibrium," meaning that  $s = f(n)$ . Because sorption or desorption in the solid region is described by a diffusion process, this assumption is valid if the characteristic time of the experiment is much longer than the characteristic time of diffusion inside the solid walls of the porous structure. If these walls have a thickness  $e$ , the characteristic time of diffusion will be  $t = (e/2)^2/4D$ . With a diffusion coefficient in the order of  $10^{-10} \text{ m}^2/\text{s}$ , and a thickness of a few microns, as for cellulose fibers, we obtain a  $t$  that is smaller than 1 s, and thus much smaller than the characteristic time of the experiments (many hours). This remains true for thicker walls of the porous medium, up to a thickness of a few millimeters, for which  $t$  reaches values in the order of hours, which, from our observations (see Discussion), is of the same order as the duration of the fastest tests. Thus, we can consider that the sorption equilibrium assumption is valid if the wall thickness is smaller than a millimeter. Note that this assumption was validated by experiments with cellulose fiber stacks of various porosities through observations of the internal MC distribution over time during desorption tests (14, 29).

With this assumption and, additionally, if during the test  $n$  remains in a linear region of the sorption curve (slope  $\alpha$ ), Equation 6 can be simplified as Equation 7:

$$\frac{\partial n}{\partial t} = -\frac{\rho_0 D^*}{\rho_s(1-\varepsilon)\alpha} \frac{\partial^2 n}{\partial x^2} \quad (7)$$

Assuming a linear regime in the sorption curve, the same equation was applied for  $s$  instead of  $n$ . Thus, transient transport in the system is described by a standard diffusion equation with a diffusion coefficient (Eq. 8):

$$D = \frac{\rho_0 D^*}{\rho_s(1-\varepsilon)\alpha} \quad (8)$$

Here, we emphasize that even if it relies on some simplification assumptions (local sorption equilibrium, linear region in the sorption curve), Equation 7 properly describes the transient processes in the material under any circumstances, with the help of the diffusion coefficient  $D$ , which is deduced from the measurement of  $D^*$ , but strongly differs from it. This shows that  $D^*$  cannot be considered as consistently describing the transport processes inside the medium under any circumstances. This describes the total vapor flux exiting the medium under steady-state conditions.

## 2.2. Boundary Conditions

We now look more precisely at the water transport processes in the air regions below and above the sample. In region C, the conditions  $n = n_i$ , with  $n_i = 0$  for a desiccant or  $n_i = 1$  for a liquid bath, are exactly reached only along the desiccant or water surface. Consequently, there is a net gradient of vapor concentration from the surface to the sample bottom, where the RH is in fact  $n = n_2$ . Such a gradient is essential as it allows the vapor to diffuse through static air between these two surfaces, otherwise there would not be any vapor flux reaching the sample bottom. From Fick's law, under isothermal conditions, we deduce that in the steady state, the gradient of vapor mass flux in this region is constant, so that the vapor flux is simply equal to Equation 9, in which  $D_0$  is the (here constant) diffusion coefficient of vapor in air.

$$J_1 = -\rho_0 D_0 \frac{(n_2 - n_i)}{h_2} \quad (9)$$

The situation is more complex in the air region above the sample. Here, the humidity is imposed by a climatic chamber or any other means that can control the RH at some distance from the sample, and adjust its value to  $n_\infty$ . This implies that air in this region is continuously renewed by air at different relative humidity. Consequently, there is an air flux along the sample surface. Finally, regardless of its characteristics, this air flux governs the boundary condition (see 29): a boundary layer forms through which the vapor at a RH  $n_1$  along the sample surface diffuses until it reaches a RH  $n_\infty$  at some distance from this surface. From a similarity analysis of the mass and momentum equations for air and vapor, it may be shown that the average outwards vapor flux along the surface can be expressed (see 29) in a straightforward way thanks to a single parameter  $\delta$ , such that (Eq. 10):

$$J_2 = -\rho_0 \frac{D_0}{\delta} (n_\infty - n_1) \quad (10)$$

in which  $\delta$  is an equivalent thickness of air through which the vapor would freely (without convection) diffuse from the material surface to a region at  $n_\infty$ , with (Eq. 11):

$$\delta = \frac{L}{F\left(\frac{\rho V L}{\mu}, \frac{\mu}{\rho D_0}, \xi\right)} \quad (11)$$

in which  $L$  is a characteristic length of the sample surface,  $\rho$ , and  $\mu$  is the air density, and viscosity,  $V$ , is a characteristic velocity of the air flux, and  $\xi$  is the surface roughness. Evidently  $\delta$  decreases when the air flux velocity increases. Finally, Equation 10 is like that employed by some authors (4, 21), and the above theory provides a full rationale for this formula and a formal expression for the unknown parameter  $\delta$ .

Note that  $\delta$  can hardly be determined a priori from the knowledge of the different characteristics of the system, i.e., the different parameters and exact geometry of the system on which  $F$  depends, as it

depends on the detailed characteristics of the flow which are complex. Instead, a simple practical approach can be recommended (see 29), which notes that  $\delta$  depends solely on the flow characteristics and can therefore be determined from the vapor flux using Equation 10, provided the RH along the sample surface is known. Let us assume that the sample, which was initially prepared at a RH  $n_0$ , is placed under a given air flux at a given RH  $n_\infty$ . In that case, the initial vapor flux is  $J_0 = \rho_0(D_0/\delta)(n_0 - n_\infty)$ . In the next step, when the RH along the sample surface has evolved to any value  $n_1$ , it follows from Equation 10 that the vapor flux can be expressed as  $J_1 = (n_1 - n_\infty)J_0/(n_0 - n_\infty)$ . This is equivalent to considering that  $\delta = \rho_0(D_0/J_0)(n_0 - n_\infty)$ . Thus, in practice, if it is possible to measure the vapor flux in the first instance, the value of  $\delta$  can be determined unambiguously. Note, however, that this approach is valid only when the air flux is imposed and constant. This cannot be used if the air flux varies depending on the current humidity via a control loop, which is likely the case in a climatic chamber. This implies that the most controlled conditions involve imposing an air flux of a given RH along the sample surface. Let us now assume that  $\delta$  has been determined. In the steady state, in the absence of a source of water vapor in the system, we have  $J_1 = J = J_2$ , which implies that, considering the new boundary conditions in terms of RH around the sample (Eq. 12):

$$J = -\rho_0 D_{eff} \frac{n_1 - n_2}{h_1} \quad (12)$$

Here  $D_{eff}$  is the (effective) diffusion coefficient associated with the vapor flow specifically through the sample.  $n_1$  and  $n_2$  can be eliminated from Equations 9, 10 and 12, yielding Equation 13:

$$J = \rho_0 D_{eff} \frac{n_i - n_\infty}{h_1} \frac{1}{1 + \frac{D_{eff} h_2 + \delta}{D_0 h_1}} \quad (13)$$

Comparing this expression with Equation 3, as obtained from the simplified approach, we deduce the following relation between the apparent diffusion coefficient and the effective one: (Eq. 14)

$$\frac{D^*}{D_{eff}} = \left(1 + \frac{D_{eff} h_2 + \delta}{D_0 h_1}\right)^{-1} \quad (14)$$

It is worth remarking that this result is independent of the values of  $n_i$  and  $n_\infty$ , which means that, for a given value of  $D_{eff}$ , the error on the diffusion coefficient by using simplified boundary conditions takes the form of a constant factor as long as the characteristics of the set up do not change (air flux, geometry). Note that when  $\delta$  is negligible compared to  $h_2$ , this expression is similar to the expression proposed in the ISO norm (3) for the relationship between the apparent and effective permeability. This allows one to conclude that the error made by using the basic approach with the simplified boundary conditions becomes significant when  $(D_{eff}/D_0)(h_2 + \delta)/h_1$  becomes larger than 0.1. The value of  $\delta$  typically ranges from approximately 1 mm for high intensity air flux, to a few centimeters for a low intensity air flux (in a "quiet room") (see 29), while  $h_1$  and  $h_2$  are typically in the order of a centimeter. This implies that the error is significant if the sample diffusivity permeability (or, equivalently, the water vapor permeability) is high, i.e., for  $D_{eff}/D_0 > 0.1$ , but it can also become significant if  $\delta$  is much larger than  $h_1$ . To minimize the potential error before any measurement, it is preferable to use a large sample thickness, a small distance  $h_2$ , and a strong air flux.

The boundary conditions also have an impact on the range of RH effectively imposed to the sample in the steady state. Under the simplified assumptions leading to Equation 3, the range covered is  $[n_i; n_\infty]$ , while in reality it is  $[n_2; n_1]$ . The deviation between these two ranges may be appreciated from the two relationships deduced from Equations 9, 10 and 12, namely, the ratio of the real to ideal range (Eq. 15) and the ratio of the deviation from the upper RH to the deviation from the lower value (Eq. 16).

$$\frac{n_2 - n_1}{n_i - n_\infty} = \frac{1}{1 + \frac{D_{eff} h_2 + \delta}{D_0 h_1}} \quad (15)$$

$$\frac{n_1 - n_\infty}{n_i - n_2} = \frac{\delta}{h_2} \quad (16)$$

It follows from **Equation 15** that the range of RH effectively covered in the sample will be significantly reduced with regard to the ideal range if the vapor diffusivity permeability through the sample and/or the ratio of the distance between the salt solution and the sample thickness are sufficiently large.

Considering the above results, the apparent diffusion coefficient of vapor through the sample, i.e.,  $D^*$ , determined from simple hypotheses, may be corrected and replaced by  $D_{eff}$  based on **Equation 14** to consider the exact boundary conditions. The total water transport diffusion coefficient through the sample, i.e.,  $D$ , is obtained from **Equation 8**, in which  $D^*$  may be replaced by  $D_{eff}$  to consider the impact of the exact boundary conditions.

### 2.3. Dynamics

We now have all the proper means for predicting the system evolution during any type of test. The mass variations of the sample over time from the very beginning of the test until the steady state are described by using **Equation 7** along with the boundary conditions given by **Equations 9** and **10**. A full comparison of this model with the experimental data is presented below. Here, it is instructive to appreciate the characteristics of typical variations expected during such an experiment with the help of an approximate approach.

For example, this is possible within the framework of our initial simplifying assumptions, i.e., for boundary conditions  $n_1 = n_\infty$  and  $n_2 = n_i$ . In our tests, the initial state of the material corresponded to a uniform distribution of  $s$  ( $s = s_0$ ), associated with a uniform distribution of  $n$  ( $n = n_0$ ). The distribution of RH over the sample thickness evolves from an initial uniform profile ( $n = n_0$ ) to a steady state profile (**Eq. 4**). In this case, **Equation 7**, with these boundary conditions, can be solved analytically (**6**) to obtain the RH distribution over time (**Eq. 17**):

$$\begin{aligned} n(x, t) = & n_i + (n_\infty - n_i) \frac{x}{h_1} \\ & + \frac{2}{\pi} \sum_{p=1}^{\infty} \frac{n_\infty \cos p\pi - n_i}{p} \sin \frac{p\pi x}{h_1} \exp(-Dp^2\pi^2 t/h_1^2) \\ & + \frac{4n_0}{\pi} \sum_{m=0}^{\infty} \frac{1}{2m+1} \sin \frac{(2m+1)\pi x}{h_1} \exp(-D(2m+1)^2\pi^2 t/h_1^2) \end{aligned} \quad (17)$$

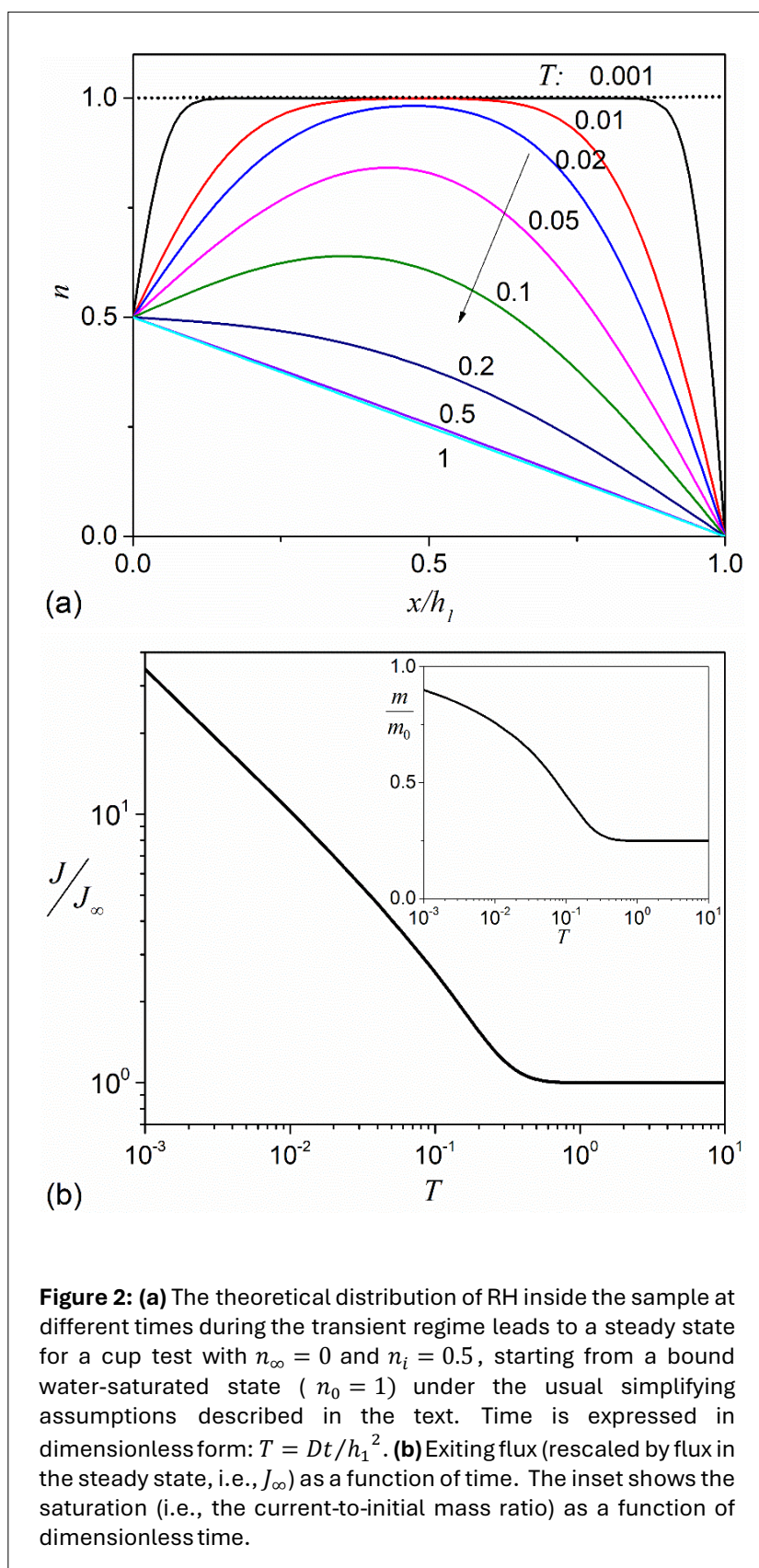
Interestingly, the mass loss of the system through the upper sample surface, which is equal to  $J = -\rho_0 D(\partial n/\partial x)_{x=h_1}$ , is readily deduced from **Equation 17**, resulting in **Equation 18**:

$$\begin{aligned} J(t) h_1 / \rho_0 D = & (n_i - n_\infty) - 2 \sum_{p=1}^{\infty} (-1)^p (n_\infty \cos p\pi - n_i) \exp(-Dp^2\pi^2 t/h_1^2) \\ & + 4n_0 \sum_{m=0}^{\infty} \exp(-D(2m+1)^2\pi^2 t/h_1^2) \end{aligned} \quad (18)$$

In this expression, the second and third terms on the right-hand side tend to zero when  $t$  approaches to infinity. In fact, because the first terms (i.e., for  $p = 1$  and  $m = 0$ ) on the right-hand side of **Equation 18** are much larger than the next ones, there is, in any case, a fast decrease in the flux, which finally reaches the steady state for a sufficiently large value of  $Dt/h_1^2$  (see **Fig. 2b**). For example, if steady state is reached when  $\exp(-D\pi^2 t/h_1^2) = 1\%$ , we obtain  $Dt/h_1^2 \approx 0.5$ . We deduce that steady state is reached at time, as shown in **Equation 19**:

$$t_c = \frac{h_1^2}{2D} \quad (19)$$

In practice, if one does not wait for a steady state, the vapor flux may be underestimated or overestimated for the wet and dry cup tests, which will lead to an incorrect evaluation of the diffusion coefficient.



### 3. DISCUSSION

#### 3.1. Materials

To illustrate and validate the aforementioned description and statement, we employed a typical hygroscopic cellulose fiber (Arbocel BC 200<sup>1</sup>) as an example to conduct sequential wet-cup tests. The cellulose fibers were strip-like in shape, with average dimensions of approximately 300  $\mu\text{m}$  in length, 10  $\mu\text{m}$  in width, and 1  $\mu\text{m}$  in thickness. The sorption curve, which reveals the bound water retention ability as a function of relative humidity, was measured by weighing the sample after it had been left for several weeks at given RH values, with the sample initially at a larger (desorption) or smaller (sorption) RH value. The tests were conducted using uncompressed cellulose fiber samples at ambient temperature (21°C). Note that under such conditions, i.e., without compression and after long periods, the data obtained after desorption or sorption are very similar (see Fig. 3). Finally, the sorption data could be well fitted with the model  $s = 0.127 \times n + (n/1.227)^{10}$ . The curve demonstrates a linear property when the moisture content remains within a specific range (see Fig. 3). Specifically, when RH is below 84%, the sorption curve can be accurately represented by the model  $s = 0.13n$ , such that  $\alpha = 0.13$ . As the RH falls within a higher range, i.e.,  $84\% < n < 100\%$ , the curve conforms to the model  $s = n - 0.73$ , so that  $\alpha = 1$ .

Recognizing that an assembly compacted from strip-like cellulose fibers can establish both a fiber network that facilitates bound water diffusion and a pore network that enables vapor diffusion, it serves as an ideal model material to represent natural cellulosic materials. Therefore, after exposure to an RH of 97% in a desiccator for several weeks, cellulose fibers were compressed into cylindrical specimens with a uniform size of approximately 5 cm in diameter and 1 cm in thickness. In this way,

we can adjust their porosity in the range of 0.33 to 0.85, which represents the diverse porosity levels found in various natural cellulosic materials. Using the cellulose density (i.e., 1500  $\text{kg m}^{-3}$ ) and assuming that the bound water has the same density as liquid water (i.e., 1500  $\text{kg m}^{-3}$ ), we deduce the apparent density of saturated fibers, and from the mass of compressed fibers and the final volume after compression, we deduce the resulting porosity of the sample. However, after releasing the piston at the end of compression, there may be some residual swelling of the structure, which must be considered to compute the effective porosity of the sample. In Table 1, we record the porosity values which were obtained in the steady state and deduced from the sample thickness. Note that this is still an average porosity, as we can expect some slight porosity variation along the sample axis owing to some pressure gradient.

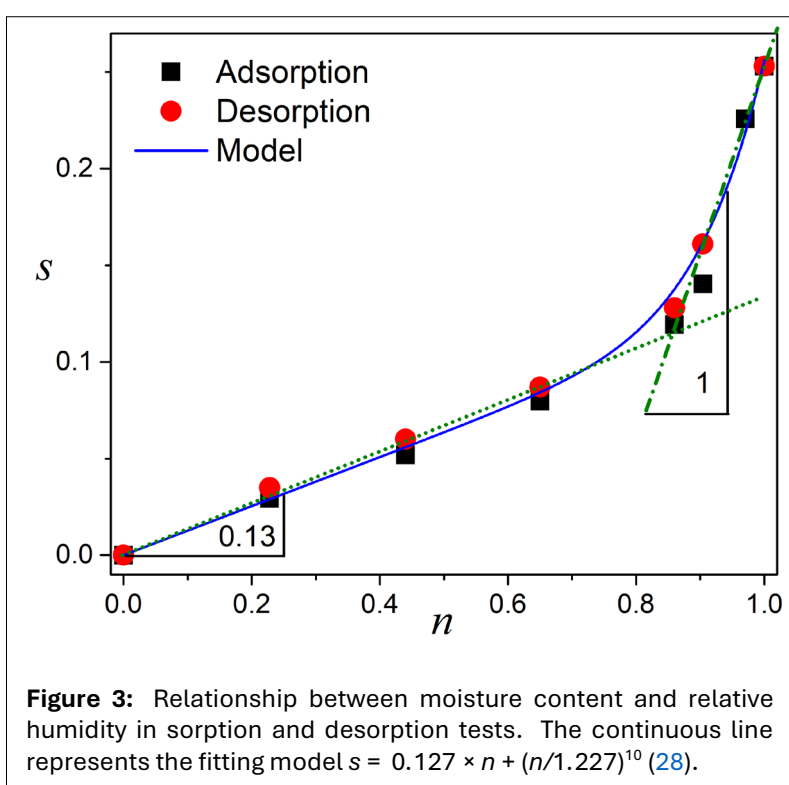


**Figure 3:** Relationship between moisture content and relative humidity in sorption and desorption tests. The continuous line represents the fitting model  $s = 0.127 \times n + (n/1.227)^{10}$  (28).

<sup>1</sup> Arbocel BC 200: Kremer Pigmente, <https://www.kremer-pigmente.com/>

**Table 1:** Main parameters of our wet-cup tests at steady state. Note that  $J_\infty$  is the (measured) vapor mass flux in the steady state.  $D^*$  was directly deduced from Equation 3 using  $J_\infty$ .  $D$  was determined by fitting the mass vs. time curve (see text).  $n_1$  and  $n_2$  were then determined from Equations 9 and 10 using the steady-state value  $J_\infty$ . Finally,  $D_{eff}$  was obtained from Equation 12 using these values for  $n_1$  and  $n_2$ .

Porosity	0.33	0.42	0.55	0.66	0.85
$h_1$ (cm)	1	1	1	1	1.05
$h_2$ (cm)	2	2	1	1	1
$n_1$	0.010	0.016	0.021	0.029	0.05
$n_2$	0.87	0.79	0.86	0.81	0.67
$s_1$	0.0012	0.002	0.0027	0.0037	0.0064
$s_2$	0.142	0.112	0.137	0.118	0.087
$J_\infty$ ( $\times 10^{-5}$ kg $m^{-2}s^{-1}$ )	0.35	0.57	0.77	1.04	1.81
$t_c$ (h)	111.1	46.3	32.7	15.4	2.9
$D^*$ ( $\times 10^{-6}$ kg $m^2/s$ )	1.75	2.85	3.84	5.19	9.00
$D_{eff}$ ( $\times 10^{-6}$ m $^2/s$ )	2.03	3.68	4.59	6.66	14.6
$D$ ( $\times 10^{-10}$ m $^2/s$ )	2.5	6	8.5	17	105

### 3.2. Experimental Procedures

As illustrated in Figure 1, we employed the typical wet-cup method to detect steady-state diffusion through the specimens. The specimen was placed above a water bath at a distance  $h_2$ , which was set at either 1 cm for samples with porosities smaller than 0.5 or 2 cm for samples with porosities higher than 0.5. The primary objective was to ensure that the moisture content over the sample remained within one linear portion of the sorption curve at a steady state. Subsequently, the sample was exposed to a vertical stream of dry air supplied from a 4 mm diameter tube at a flow rate of 10 L/min. The sample was placed in a 5 cm diameter cylinder to seal the lateral surfaces, ensuring one-dimensional diffusion through the sample.

The entire system was then placed on a balance to monitor the overall weight evolution over time, with measurements recorded every second. We then averaged the data over 2-minute intervals, and displayed only one out of every approximately 25 resulting values in the graphs to avoid clutter and ensure readability. This data treatment approach allows the reduction of scattering due to mass fluctuations caused by ambient environmental disturbances, while maintaining the accuracy of the observed mass evolution over time. Note that the air flux induces additional pressure that affects the apparent weight of the system recorded by the balance; however, this perturbation is constant and cannot impact the observations of interest, as we are primarily focused on the apparent mass variation (mass loss) over time from the initial time at which the constant air flux is applied.

To maintain consistency, the outlet of the dry air was set at a constant distance of 4 cm from the surface of the specimen for each test, resulting in a boundary condition expressed in Equation 10, with a  $\delta$  value of 1.5 mm. This value was deduced from the initial drying rate when the relative humidity along the surface remained at 1 (from independent tests with a sample filled with liquid water (see 29)). Recall that the value of  $\delta$  results from an average of the local boundary layer characteristics along the sample surface (29); typically, the local value for this thickness increases with the distance covered by the air flux along the surface. Here, we used a vertical air flux rather than a tangential air flux to limit the heterogeneity of the boundary layer thickness along the surface. Indeed, the flux penetration into the sample is negligible here, owing to the much lower permeability of this cellulosic specimen compared to that of the container above its surface, and the fact that the paths along the longitudinal axis of the sample are dead ends due to the presence of the container bottom. Thus, such an air flux invariably results in a local tangential flow along the sample surface. Finally, the heterogeneity of the boundary layer characteristics along the sample surface is limited due to the smaller length of variation (along the

sample radius instead of the sample diameter), and the complex air recirculation process that results from such conditions. We expect that the bottom water bath and the top imposed dry air collectively induce one-dimensional diffusion along the thickness (longitudinal axis) of the specimen. Throughout the process, experimental data on the mass loss of the system through the upper sample surface versus time (i.e., mass loss vs. time) were recorded on a scale and stored on a connected PC for subsequent analysis.

### 3.3. Numerical simulation

First, we review the comprehensive model and boundary conditions to simulate the vapor diffusion process through the sample in the wet-cup system in the transient regime up to the steady state. **Equation 7** represents the complete vapor diffusion model along the thickness of the cellulose sample and **Equation 10** corresponds to the boundary condition at the top open surface. The boundary condition for RH at the bottom surface of the cellulose sample ( $x = 0$ ) (see **Fig. 1**) adheres to the principles of continuity and mass balance (**Eq. 20, Eq. 21**):

$$(n)_{x=0^-} = (n)_{x=0^+} \quad (20)$$

$$D_0 \left( \frac{\partial n}{\partial x} \right)_{x=0^-} = D^* \left( \frac{\partial n}{\partial x} \right)_{x=0^+} \quad (21)$$

The vapor diffusion in the void space between the water bath and cellulose sample follows a typical vapor diffusion model in the air (**Eq. 22**):

$$\frac{\partial n}{\partial t} = D_0 \frac{\partial^2 n}{\partial x^2} \quad (22)$$

The surface of the water bath established a fixed boundary condition, maintaining the RH at a constant value of 1. With a specified initial condition, the complete diffusion models applied in the wet cup test can be solved using a suitable numerical algorithm. Any finite element software, such as the commercial software COMSOL Multi-physics or the popular open-source computing platform FEniCSx, can be used to solve the governing models. Here, the governing equations are discretized in space using the finite element method and in time, employing an implicit time-stepping method, specifically the backward Euler method. The mesh was designed to be sufficiently refined, optimizing the computing time while maintaining a small size to capture the fields accurately. More specifically, a boundary layer refinement near the interface and top surface was employed. The maximum element size (length) throughout the system is 0.04 cm. To ensure the accuracy of our results, we conducted additional simulations using finer grids and compared the key output parameters. The results showed minimal changes, confirming that our results are independent of further grid refinement. Furthermore, to enhance the efficiency of solving the governing equations, the time step was adaptively adjusted based on the convergence rate. This approach ensures both computational efficiency and an accurate representation of the diffusion process in the wet-cup test. Upon solving the models, the mass loss versus time curves were obtained through the time integral of the mass flux at the upper open surface.

### 3.4. Theory vs. experiment

The experimental data of mass loss versus time are shown in **Figure 4** for both the low-porosity (**Fig. 4a**) and high-porosity samples (**Fig. 4b**). All the mass loss curves were characterized by an initial rapid decline followed by a gradual decrease until a steady state was achieved, characterized by a constant slope of the mass loss versus time.

Because we are dealing with transient tests, we must use **Equation 7** (with the diffusion coefficient  $D$ ) with the boundary conditions from **Equations 9** and **10**. Notably, the application of a single, assuming a constant global diffusion coefficient ( $D$ ), the only fitting parameter in the simulation, generates predicted mass loss curves (solid lines in **Fig. 4**) that align remarkably well with the corresponding experimental data at any time up to the steady state and for various porosities (with different values for  $D$ ). This suggests that for each porosity, the chosen coefficient successfully encompasses the intricate

diffusion dynamics, irrespective of moisture content variations. However, it is worth recalling that this conclusion applies to experimental conditions that, at least in steady state, preserve MC values in a range for which the sorption curve can be well represented by a straight line (see below). It is beyond the scope of the present work to study more precisely, through systematic experiments of that type under different boundary conditions, the potential variations in the diffusion coefficient needed to represent the data.

From the simulation, key parameters at steady state, such as  $n_1$ ,  $n_2$ , and  $J$ , were determined. It appears that  $n_1$  closely approaches  $n_\infty$  (i.e., 0) owing to the small value of  $\delta$ . Conversely, the RH at the bottom of the cellulose sample ( $n_2$ ) deviated from  $n_i = 1$  and was approximately 0.84 or less. Based on the values of  $n_1$  and  $n_2$ , the linear characteristics of the sorption curves, and the sorption equilibrium assumption, the corresponding RH value remained within the linear sorption region over the sample. This supports the validity of the linear sorption assumption and the equilibrium condition between vapor and moisture content over the cellulose sample at a steady state.

The dashed lines in **Figure 4** are placed at the theoretical time ( $t_c$ )

to reach a steady state for each experiment according to **Equation 19**, using the diffusion coefficient ( $D$ ) employed in the simulation. Although it is difficult to determine a precise value corresponding to the transition to steady state, the theoretical prediction of this time (under simplified assumptions) provides a good estimate of the experimental time for this transition (see **Fig. 4**). The theoretical bound water distribution over time for the experiments in **Figure 4b** is shown in the **Supplementary Material** (available online). We can see that the evolution of these distributions is similar, but with different dynamics, and the steady-state distribution is approximately reached for  $t_c$ . This agreement suggests that the chosen constant diffusion coefficient accurately captures the mass loss over time and provides an effective estimate of the time required for the system to achieve a steady state. Recall that waiting for steady state is essential, as deviating from this condition could lead to an overestimation of vapor

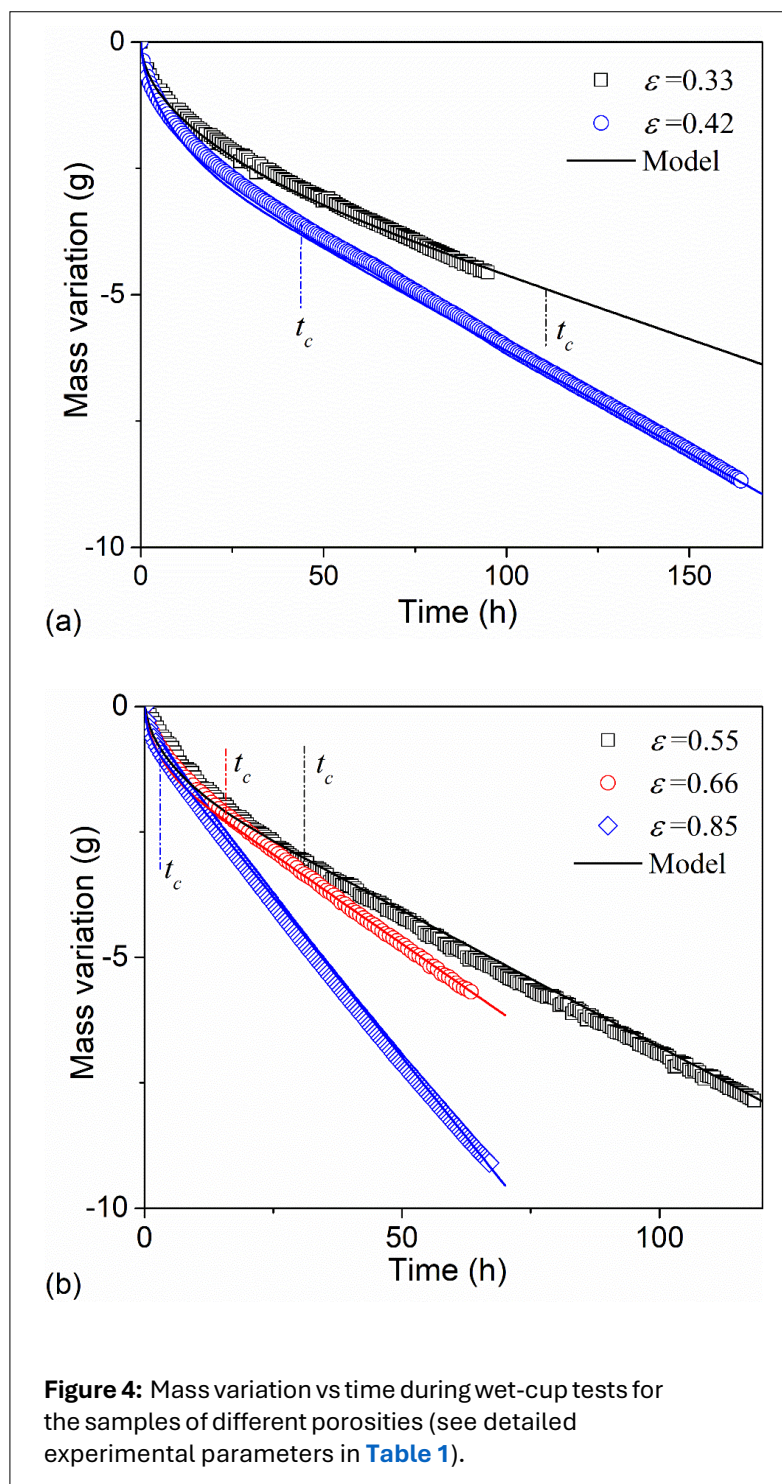


**Figure 4:** Mass variation vs time during wet-cup tests for the samples of different porosities (see detailed experimental parameters in **Table 1**).

flux, consequently inflating the deduced diffusion coefficient value. Consequently, the above agreement suggests that a critical operation would consist of checking a posteriori the validity of the chosen time for considering in practice that steady state has been reached by comparing this time with the value deduced from [Equation 19](#) with the diffusion coefficient deduced from [Equations 3](#) and [8](#).

With the help of our detailed simulation results that provide all the characteristics of the transport, including  $n_1$  and  $n_2$ , we can now examine the values of the apparent diffusion coefficients ( $D^*$  and  $D_{eff}$ ), which can be deduced from the standard approach ([Eq. 3](#), [Eq. 12](#)) (see [Table 1](#)). The noticeable discrepancy between  $D^*$  and  $D_{eff}$  primarily arises because of the decrease in the RH in region C, where  $n_i$  transitions from a higher value to  $n_2$ . This difference is particularly evident in high-porosity samples characterized by greater permeability, and thus a larger  $D_{eff}$  value. This observation underscores the significance of maintaining a small ratio between the distance from the salt solution and sample thickness for precise diffusion coefficient measurements. Additionally, the more pronounced deviation in high-porosity samples under the same experimental conditions highlights the necessity of a meticulous experimental design that considers the specific permeable characteristics of the sample to ensure accurate measurements.

Note that all the present approaches correspond to desorption conditions; for the tests, the sample was initially saturated with bound water, so that a gradient of moisture content progressively developed during the test. The approach might need to be modified to consider possible different sorption dynamics or equilibria for compressed samples if the tests were conducted with samples in an initially dry state, a situation that would involve sorption processes.

## 4. CONCLUSION

In this study, we revisited the wet cup test ([2](#), [3](#)) and its interpretation in the context of its application to a hygroscopic material. First, we presented explicit relationships for properly considering the boundary conditions. This led to full quantification of the error when considering  $D^*$  instead of  $D_{eff}$  (obtained after appropriate corrections) as the apparent vapor diffusion coefficient. We also precisely identified the conditions under which one can consider that a steady state is reached, which is critical for the determination of  $D_{eff}$ . However, the primary issue with these tests is the physical interpretation of the obtained parameter  $D_{eff}$ . It is essential to recognize a fundamental distinction between  $D_{eff}$ , the diffusion coefficient deduced under the assumption of a non-hygroscopic material, and  $D$ , the total water transport diffusion coefficient inside the material considering the material's hygroscopicity. Indeed, the transportation of moisture within hygroscopic bio-based materials is intricate, encompassing not only vapor diffusion in the pore network, but also bound water diffusion through the fiber network and exchange between the two phases. In such systems, as a first approximation, transient transport follows a standard diffusion ([Eq. 7](#)) with diffusion coefficient  $D$ , which is proportional to  $D_{eff}$  via a factor that depends on the porosity of the material. This distinction is pivotal, underscoring the fact that  $D_{eff}$  cannot be uniformly regarded as a consistent descriptor of transport processes within the medium under all circumstances. While  $D_{eff}$  provides valuable insights into the steady-state vapor flux exiting the material under the specific experimental conditions chosen, the adoption of a standard diffusion coefficient  $D$  becomes imperative to capture the complexity of transient transport, accounting for both vapor and bound water diffusion through the fiber network and allowing the prediction of vapor diffusion through the material under any condition.

## STATEMENTS AND DECLARATIONS

### Supplementary Material

Supplementary Material is available online [here](#).

### Acknowledgements

The Views and opinions expressed are those of the authors only, and do not necessarily reflect those of the European Union or the European Research Council. Neither the European Union nor the granting authority can be held responsible for them.

### Author Contributions

Y.Z. and E.M. conducted the experiments and analyzed the data. Y.Z., L.B. and P.C. developed the theory. Y.Z., L.B., and P.C. prepared the manuscript. All authors reviewed the manuscript.

### Conflicts of Interest

The authors declare that they have no conflicts of interest.

### Funding Received

Funded by the Labex MMCD, provided by the national program Investments for the Future of the French National Research Agency (ANR-11-LABX-022), and co-funded by The European Union (ERC PHYSBIOMAT - 101095764).

### ORCID IDs

Yuliang Zou

 <https://orcid.org/0000-0002-4822-296X>

Eléa Moss

 <https://orcid.org/0009-0006-1699-3221>

Laurent Brochard

 <https://orcid.org/0000-0001-9853-1827>

Philippe Coussot

 <https://orcid.org/0000-0003-3980-0825>

## REFERENCES

1. Amziane, S., & Collet, F. (2017). Bio-aggregates based building materials: State-of-the-Art Report of the RILEM Technical Committee 236-BBM (Vol. 23). Springer. <https://doi.org/10.1007/978-94-024-1031-0>
2. ASTM. (1989). Standard test methods for water vapor transmission of materials (Standard No. ASTM E96-80). American Society for Testing and Materials. Philadelphia, United States.
3. BSI. (2016). Hygrothermal performance of building materials and products-determination of water vapour transmission properties. Cup method (Standard No. ISO 12572:2016). British Standards Institution. London, UK. <https://doi.org/10.3403/30294357>
4. Colinart, T., & Glouannec, P. (2022). Accuracy of water vapor permeability of building materials reassessed by measuring cup's inner relative humidity. *Building and Environment*, 217, 109038. <https://doi.org/10.1016/j.buildenv.2022.109038>
5. Collet, F., Chamoin, J., Pretot, S., & Lanos, C. (2013). Comparison of the hygric behaviour of three hemp concretes. *Energy and Buildings*, 62, 294–303. <https://doi.org/10.1016/j.enbuild.2013.03.010>
6. Crank, J. (1979). The mathematics of diffusion. Oxford University Press.
7. Desta, T. Z., Langmans, J., & Roels, S. (2011). Experimental data set for validation of heat, air and moisture transport models of building envelopes. *Building and Environment*, 46(5), 1038–1046. <https://doi.org/10.1016/j.buildenv.2010.11.002>
8. Dubois, S., Evrard, A., & Lebeau, F. (2014). Modeling the hygrothermal behavior of biobased construction materials. *Journal of Building Physics*, 38(3), 191–213. <https://doi.org/10.1177/1744259113489810>
9. French Ministry. (2021). Matériaux de construction biosourcés et géosourcés [Bio and geo-sourced building materials]. <https://www.ecologie.gouv.fr/materiaux-construction-biosources-et-geosources>
10. Grammatikos, S., Riley, M., Bras, A., et al. (2021). Analysis of dynamic moisture movement within bio-based earth mortars. *Construction and Building Materials*, 306, 124862. <https://doi.org/10.1016/j.conbuildmat.2021.124862>
11. Jones, D., & Brischke, C. (Ed.) (2017). 5 - Performance of the bio-based building materials. In: Performance of Bio-based Building Materials. Woodhead Publishing. 249-333. <https://doi.org/10.1016/b978-0-08-100982-6.00005-7>

12. Le, A. T., Maalouf, C., Mai, T. H., Wurtz, E., & Collet, F. (2010). Transient hygrothermal behaviour of a hemp concrete building envelope. *Energy and Buildings*, 42(10), 1797–1806. <https://doi.org/10.1016/j.enbuild.2010.05.016>
13. Li, Y., Fazio, P., & Rao, J. (2012). An investigation of moisture buffering performance of wood paneling at room level and its buffering effect on a test room. *Building and Environment*, 47, 205–216. <https://doi.org/10.1016/j.buildenv.2011.07.021>
14. Ma, X., Maillet, B., Brochard, L., Pitois, O., Sidi-Boulenouar, R., & Coussot, P. (2022). Vapor-sorption Coupled Diffusion in Cellulose Fiber Pile Revealed by Magnetic Resonance Imaging. *Physical Review Applied*, 17(2), 024048. <https://doi.org/10.1103/physrevapplied.17.024048>
15. Mnasri, F., Abahri, K., El, G. M., Bennacer, R., & Gabsi, S. (2017). Numerical analysis of heat, air, and moisture transfers in a wooden building material. *Thermal Science*, 21(2), 785–795. <https://doi.org/10.2298/tsci160421248m>
16. Mustapha, R., Zoughaib, A., Ghaddar, N., & Ghali, K. (2020). Modified upright cup method for testing water vapor permeability in porous membranes. *Energy*, 195, 117057. <https://doi.org/10.1016/j.energy.2020.117057>
17. Olutimayin, S. O., & Simonson, C. J. (2005). Measuring and modeling vapor boundary layer growth during transient diffusion heat and moisture transfer in cellulose insulation. *International Journal of Heat and Mass Transfer*, 48(16), 3319–3330. <https://doi.org/10.1016/j.ijheatmasstransfer.2005.02.024>
18. Osanyintola, O. F., & Simonson, C. J. (2006). Moisture buffering capacity of hygroscopic building materials: Experimental facilities and energy impact. *Energy and Buildings*, 38(10), 1270–1282. <https://doi.org/10.1016/j.enbuild.2006.03.026>
19. Petersen, D., Link, R., & Kumaran, M. (1998). An Alternative Procedure for the Analysis of Data from the Cup Method Measurements for Determination of Water Vapor Transmission Properties. *Journal of Testing and Evaluation*, 26, 575–581. <https://doi.org/10.1520/jte12115j>
20. Remki, B., Abahri, K., Tahlaiti, M., & Belarbi, R. (2012). Hygrothermal transfer in wood drying under the atmospheric pressure gradient. *International Journal of Thermal Sciences*, 57, 135–141. <https://doi.org/10.1016/j.ijthermalsci.2012.02.005>
21. Seng, B., Magniont, C., & Lorente, S. (2019). Characterization of a precast hemp concrete block. Part II: Hygric properties. *Journal of Building Engineering*, 24, 100579. <https://doi.org/10.1016/j.jobbe.2018.09.007>
22. Trechsel, H. R. (1994). Moisture control in buildings. *ASTM International*.
23. Wang, X., Jin, X., Yin, Y., Wang, X., Shi, X., & Zhou, X. (2020). Study on non-isothermal moisture transfer characteristics of hygroscopic building materials: From parameter characterization to model analysis. *Energy*, 212, 118788. <https://doi.org/10.1016/j.energy.2020.118788>
24. Woloszyn, M., Kalamees, T., Abadie, M. O., Steeman, M., & Kalagasidis, A. S. (2009). The effect of combining a relative-humidity-sensitive ventilation system with the moisture-buffering capacity of materials on indoor climate and energy efficiency of buildings. *Building and Environment*, 44(3), 515–524. <https://doi.org/10.1016/j.buildenv.2008.04.017>
25. Woloszyn, M., & Rode, C. (2008). Tools for performance simulation of heat, air and moisture conditions of whole buildings. *Building Simulation*, 1, 5–24. <https://doi.org/10.1007/s12273-008-8106-z>
26. Yoshino, H., Mitamura, T., & Hasegawa, K. (2009). Moisture buffering and effect of ventilation rate and volume rate of hygrothermal materials in a single room under steady state exterior conditions. *Building and Environment*, 44(7), 1418–1425. <https://doi.org/10.1016/j.buildenv.2008.09.007>
27. Zou, Y., Maillet, B., Brochard, L., & Coussot, P. (2023). Fast transport diffusion of bound water in cellulose fiber network. *Cellulose*, 30(12), 7463–7478. <https://doi.org/10.1007/s10570-023-05369-4>
28. Zou, Y., Maillet, B., Brochard, L., & Coussot, P. (2024). Unveiling moisture transport mechanisms in cellulosic materials: Vapor vs. bound water. *PNAS nexus*, 3(1), pgad450. <https://doi.org/10.1093/pnasnexus/pgad450>
29. Zou, Y., Yan, L., Maillet, B., Sidi-Boulenouar, R., Brochard, L., & Coussot, P. (2023). Critical role of boundary conditions in sorption kinetics measurements. *Langmuir*, (51), 18866–18879. <https://doi.org/10.1021/acs.langmuir.3c02729>